Melanoblast proliferation dynamics during mouse embryonic development: Modeling and validation

Bouchra Aylaj, Flavie Luciani, Veronique Delmas, Lionel Larue, Florian de Vuyst

www.elsevier.com/locate/yjtbi

Melanoblast proliferation dynamics during mouse embryonic development: Modeling and validation

Bouchra Aylaj, Flavie Luciani, Veronique Delmas, Lionel Larue, Florian De Vuyst

PII: S0022-5193(11)00067-1
DOI: doi:10.1016/j.jtbi.2011.01.041
Reference: YJTBI 6353

To appear in: *Journal of Theoretical Biology*

Received date: 28 February 2010
Revised date: 1 January 2011
Accepted date: 25 January 2011

Cite this article as: Bouchra Aylaj, Flavie Luciani, Veronique Delmas, Lionel Larue and Florian De Vuyst, Melanoblast proliferation dynamics during mouse embryonic development: Modeling and validation, *Journal of Theoretical Biology*, doi:10.1016/j.jtbi.2011.01.041

Melanoblast proliferation dynamics during mouse embryonic development. Modeling and Validation

Bouchra Aylaj[a,*], Flavie Luciani[b], Veronique Delmas[b], Lionel Larue[b], Florian De Vuyst[a,c,d]

[a] *Laboratoire Mathématiques Appliquées aux Systèmes, Ecole Centrale Paris, Grande Voie des Vignes, 92295 Châtenay-Malabry cedex, France*
[b] *Developmental Genetics of Melanocytes, Centre National de la Recherche Scientifique (CNRS) 3347 - Institut Curie, 91405 Orsay Cedex, France*
[c] *Centre de Mathématiques et de leurs applications, Ecole Normale Supérieure de Cachan, 61, avenue du Président Wilson, 94235 Cachan cedex, France*
[d] *Energy Conversion Research Center, Doshisha University, 1-3 Tatara-Miyakodani, Kyotanabe 610-0394, Japan*

Abstract

In this paper, we are looking for mathematical modeling of mouse embryonic melanoblast proliferation dynamics, taking into account, the expression level of β-catenin. This protein plays an important role into the whole signal pathway process. Different assumptions on some unobservable features lead to different candidate models. From real data measured, from biological experiments and from a priori biological knowledge, it was able to validate or invalidate some of the candidate models. Data assimilation and parameter identification allowed us to derive a mathematical model that is in very good agreement with biological data. As a result, the produced model can give tracks for biologists into their biological investigations and experimental evidence. Another interest is the use of this model for robust hidden parameter identification like double times or number of founder melanoblasts.

Keywords: melanoma, β-catenin, doubling time, data assimilation, variational approach.

*Address correspondence to Bouchra AYLAJ
E-mail: bouchra.aylaj@gmail.com
Tel: +33 (0)2 23 48 51 98
Fax: +33 (0)2 23 48 51 80
INRA - UMR 1099 BIO3P, Centre INRA de Rennes, Equipe Epidémiologie, Sol et Systèmes (EPSOS), Domaine de la Motte, BP 35327, 35653 Le Rheu cedex -FRANCE

Email addresses: bouchra.aylaj@gmail.com (Bouchra Aylaj), flavie.luciani@curie.fr (Flavie Luciani), veronique.delmas@curie.fr (Veronique Delmas), lionel.larue@curie.fr (Lionel Larue), devuyst@cmla.ens-cachan.fr (Florian De Vuyst)

Nomenclature

n_d	total number of melanoblasts in dermis
$n_d(t)$	total number of melanoblasts in dermis at time t
$n_{d/s}$	total number of melanoblasts in dermis per section
$n_{e/s}$	total number of melanoblasts in epidermis per section
n_e	total number of melanoblasts in epidermis
Φ	flux of melanoblasts from dermis to epidermis
$n = n_d + n_e$	total population of melanoblasts
$y_d = y = \frac{n_d}{n_d+n_e}$	fraction of melanoblasts in dermis
$y_e = 1 - y = \frac{n_e}{n_d+n_e}$	fraction of melanoblasts in epidermis
$\kappa(t)$	factor coefficient of the flux Φ at time t ($\kappa(t) \geq 0$)
$\tau_d(t)$	doubling time in dermis at time t
$\tau_e(t)$	doubling time in epidermis at time t
$\mu_d(t) = \frac{\log(2)}{\tau_d(t)}$	growth rate in dermis at time t
$\mu_e(t) = \frac{\log(2)}{\tau_e(t)}$	growth rate in epidermis at time t
N_m	number of embryonic day measurements

1. Introduction

Tumor progression is a multistep process in which genetic modification occur and influence proliferation rates. The importance of examining the genetic mutations in cancer development is emphasized in [6]. The mathematical literature has been devoted to modeling gene interactions and their evolution. Two mathematical approaches are examined in [1], the first one is due to Komarova [10, 11] while the second one is by Gatenby [5]. The first approach in [10, 11] is focused on the stochastic dynamics of gene interaction in cancer initiation and progression related to mutations which generate loss and gain of function. Gatenby and Vincent adopted a game theory approach heavily influenced by population dynamics to investigate the influence of the tumour-host interface in colorectal carcinogenesis [5] and suggest therapeutic strategies. Moreover, several authors have proposed various models of the macroscopic behavior cancer tissues, for example, the paper [2] is focused on the modeling and simulation of large systems of interacting entities whose microscopic state includes not only geometrical and mechanical variables, but also biological functions. The systems of partial differential equations can be used to model large systems of interacting cells whose microscopic state includes internal variables related to biological functions. An introduction to population dynamics with internal structure is given in [20]. Mathematical models can provide biologists and clinicians with tools that might guide their efforts to elucidate fundamental mechanisms of cancer initiation and progression and either improves current treatment strategies or stimulates the development of new

ones. Mathematical models plays significant role for better understanding of evolutionary concepts such as mutation and selection [14]. One of the main purposes of this study is, being based on developed early models and experiment data, to propose a new mathematical model. This paper will be led in the context of understanding of the melanocytes cancerisation mechanisms in melanomas. The skin melanomas can be very aggressive and often display multi-drug-resistance characteristics. Molecular and cellular mechanisms occurring during embryonic development. For this purpose, we start with the definition of the melanoblast during embryonic development.

1.1. Biological context

Melanoma, like other cancers, often presents constitutive activation of the wnt signaling pathway as evidenced by nuclear accumulation of β-catenin. A usual biological "mirror" model for the understanding of melanoma cancer dynamics is the migration and proliferation dynamics of melanoblasts, during embryonic development, can be colored and counted during biological experiments [3, 16, 22]. In [3, 12], it was shown that β-catenin reduces the number of melanoblasts in vivo.

As a complementary study to [3, 12], it is intended to estimate melanoblast doubling times into dermis and epidermis according to the activity of β-catenin.

To this goal, a mathematical model of mouse embryo melanoblast proliferation dynamics is needed. This is the aim of this paper. In this model, the total number of melanoblasts in the dermis n_d and the total number of melanoblasts in the epidermis n_e with fluxes between themselves have to be considered.

A priori biological knowledge helps us to design and reduce the set of admissible models. Experimental measurements can help for:

1. quantitative model closure;
2. validation of the mathematical model;
3. numerical robust identification of hidden parameters.

On the other hand, the macroscopic understanding of the dynamics is not fully understood and assumptions have to be done. From the experimental point of view, melanoblasts can be colored and then counted at some instants between embryonic days E10.5 and E15.5. However, these data generally are subject to some uncertainty due to the measurements errors or human error during counting process. Moreover, some important features of the dynamics are unobservable. This is the case for example for the melanoblast flux from dermis to epidermis because the biological measurements are performed at fixed instants.

1.2. Biological assumptions

Founder melanoblasts appear at embryonic day E8.5 from the neural tube in the dermis. The melanoblasts then proliferate and migrate into the dermis dorso laterally to the somites up to the belly. The biological data presented by Luciani et al. (submitted for publication). From E11.5, melanoblast start to cross the epidermis membrane matrix with a flux rate Φ and begin to invade the epidermis. In parallel, they continue to proliferate. Biological observations allow us to assume that there is no transdifferentiation between melanoblasts and other cells and that apoptosis is negligible.

Consequently, from an initial number of founder melanoblasts at E8.5, the biological model (melanoblasts in dermis/melanoblasts in epidermis) is governed by the proliferation and flux between dermis and epidermis without any exogenous exchanges at the system boundary. Finally, it is biologically reasonable to think that there is no flux from the epidermis to the dermis. Basic statistics on measurements and biological knowledge are able to give lower and upper bounds, i.e. a confidence interval for the doubling times τ_d and τ_e in dermis and epidermis respectively. However, there is neither knowledge nor experimental evidence of bounds for the epidermis flux rate Φ. The biological model considered here is summarized in Figure 1.

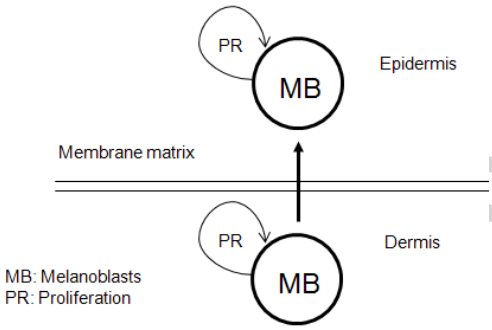

Figure 1: Definition of biological model

After the above preliminaries, this paper, is organised as follows: the determination and the illustration of biological data, which are the subject of the mathematical modelling approache, are given in Section 2. In Section 3, we consider different mathematical model candidates for the proliferation dynamics. The equivalent form of the mathematical model without dependency on doubling times is given in Section 4, this section deals with existence, uniqueness and behavior of solutions, in particular, the estimates for stability of solution with respect to the model parameters. The section 5, deals with the numerical estimation of initial fraction and number of founder melanoblasts in dermis. From biological BrdU consideration, the coarse estimation of doubling times is given in Section 6. Section 7 proposes a critical analysis related to estimate the states of the biological systems and parameters in the model. Section 8 is reserved for conclusions and research perspectives.

2. Biological measurements and first stage of data processing

2.1. Setup and methodology for mean values and standard deviations

There are two types of biological data:

1. Number of melanoblasts estimated from Whole Mount data: it is a visual counts on the both sides of a mouse. From E10.5 to E15.5 embroyonic days, the total number of melanoblasts embryos is shown in [3].

2. Number of melanoblasts estimated from transversal section of embryos : it is a visual counts by section of about 7 microns. It shows the visibility of melanoblasts number in dermis i.e. $n_{d/s}$ and epidermis i.e. $n_{e/s}$.

The expression of total number of melanoblasts in dermis i.e. n_d (resp. epidermis i.e. n_e) was calculated using the average number of whole mount data i.e. n multiplied by number of fraction per section of melanoblasts in dermis (resp. epidermis), i.e

$$n_d = n\,\frac{n_{d/s}}{n_{d/s}+n_{e/s}}, \quad n_e = n\,\frac{n_{e/s}}{n_{d/s}+n_{e/s}}. \tag{1}$$

By similar considerations, we can also calculate the standard deviations relative to the total number of melanoblasts.

An m^d (resp. m^e)-dimensional values of melanoblasts N_d (resp. N_e) in dermis (resp. epidermis), given by Fig. (2). N_d^j and N_e^j are given by expressions (1), for all $j = 1, ..., m^d$ (resp. $j = 1, ..., m^e$).

The sample mean n_d (resp. n_e) of melanoblasts in dermis (resp. epidermis), and the standard deviation are shown in Tab. (1)-(3), with covariance matrix Q_d, (resp. Q_e):

$$n_d = \frac{1}{m^d}\sum_{j=1}^{m^d} N_d^j, \qquad n_e = \frac{1}{m^e}\sum_{j=1}^{m^e} N_e^j,$$

$$Q_d = \frac{1}{m^d-1}\sum_{j=1}^{m^d}(N_d^j - n_d)(N_d^j - n_d)^T, \qquad Q_e = \frac{1}{m^e-1}\sum_{j=1}^{m^e}(N_e^j - n_e)(N_e^j - n_e)^T.$$

2.2. Data plots

Illustrations of biological data are given in Fig (3)-(5), on wild type (WT) mice and $bcat^{sta}$ and del^{ex26} mutant mice respectively.

It is noted that the plots for WT and bcat^{sta} mice look very similar. The melanoblasts population in epidermis exponentially grows. Between E12.5 and E14.5 there is a decrease of the number of melanoblasts in dermis due either of the decrease of the growth rate or an important flux into epidermis.

2.3. Feature extraction from biological data

2.3.1. Total number of melanoblasts

For modeling, it is important to reveal some features of the biological data. On figure 6, the history of the logarithm of the total number of melanoblasts (dermis+epidermis) is plotted for Wild type mice (WT), $bcat^{sta}$ mutants and del^{ex26} mutants.

Circles represent measurements. The plots are also extended to the embryonic day E8.5 by an expected value of the number of melanoblasts. It is biologically known that β-catenin pathway cannot act before embryonic day E10.5, so that the same value

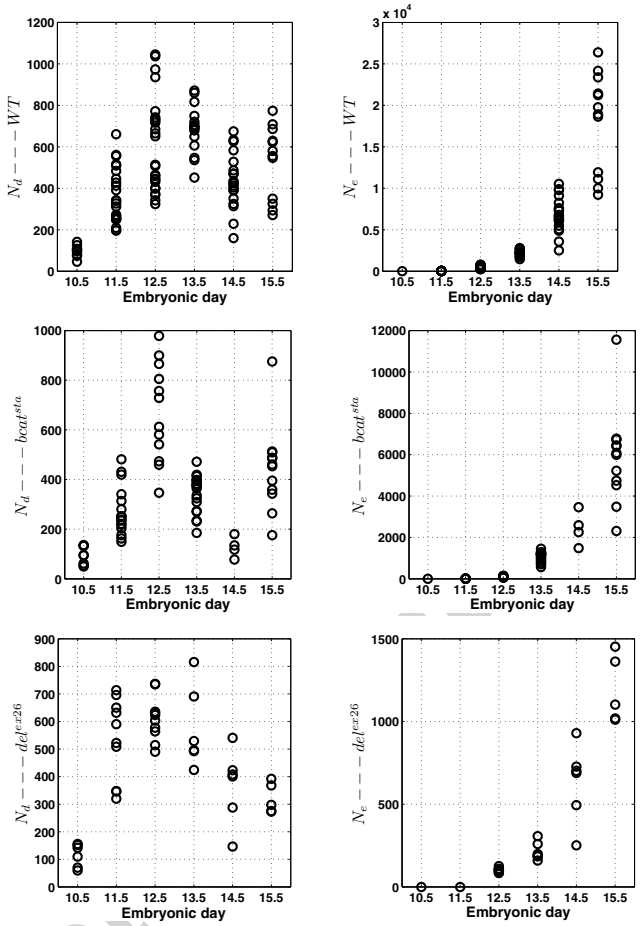

Figure 2: History of Number of Melanoblasts in both dermis and epidermis for three mice types.

is taken for the three types of mice. At day E8.5, it is biologically expected that the number of precursor melanoblasts is in the range $[10, 30]$. To extend the data, we used an initial number of melanoblasts equal to 16. What it is observed is that the plots for WT and $bcat^{sta}$ can be well approximated by a line, showing an exponential growth for the total number of cells. For del^{ex26} mutants, the behaviour is quite different, showing a fast growth between E8.5 and E11.5 and a slower growth between E11.5 and E15.5 with can be linearly regressed in log scale.

*2.3.2. Fractions of melanoblasts in dermis (*resp. epidermis)

On figure 7, the fractions of melanoblasts in dermis y and epidermis $(1 - y)$ is plotted for each of the mice. It appears that the fractions have a S-shaped profile

E. day	Mean nb mel. in dermis	Std dev nb mel. in dermis	Mean nb mel. in epidermis	Std dev nb.mel. in epidermis
E10.5	98	28.49	0	0
E11.5	366.73	118	26.04	24.37
E12.5	605.96	213.61	455.95	180.02
E13.5	684.83	164.74	2189.03	326.77
E14.5	436.77	211.20	6822.02	1415.15
E15.5	528.63	725.49	18014.03	5397.44

Table 1: Mean values and standard deviations from experimental measurements on wild type (WT) mice.

E. day	Mean nb mel. in dermis	Std dev nb mel. in dermis	Mean nb mel. in epidermis	Std dev nb.mel. in epidermis
E10.5	95	36.58	0	0
E11.5	271.81	87.58	5.71	10.59
E12.5	670.65	173.77	102.67	54.30
E13.5	343.93	83.12	1058.37	222.45
E14.5	127.39	87.19	2451.10	772.88
E15.5	443.45	377.82	5858.37	2058.85

Table 2: Mean values and standard deviations from experimental measurements on $bcat^{sta}$ mutant mice for both dermis and epidermis.

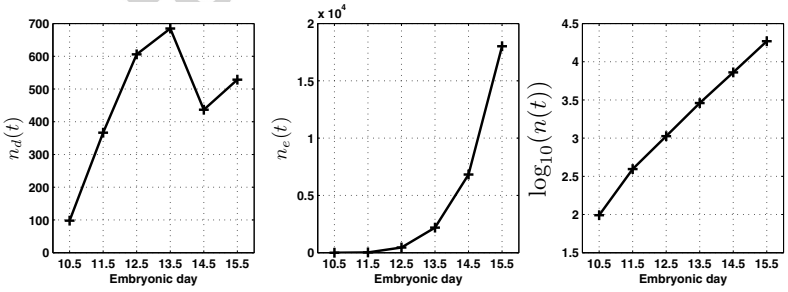

Figure 3: History of melanoblasts for WT mice. From left to right: $n_d(t)$, $n_e(t)$ and $\log_{10}(n(t))$.

revealing an underlying "logistic" differential equation on the cell fraction y which is a common feature for the three mice. One can also observe a slight difference between

E. day	Mean nb mel. in dermis	Std dev nb mel. in dermis	Mean nb mel. in epidermis	Std dev nb.mel. in epidermis
E10.5	106	38.17	0	0
E11.5	532.6	149.58	0	0
E12.5	611.13	76.65	104.06	18.50
E13.5	574.71	153.17	215.95	49.96
E14.5	367.74	177.21	632.25	189.80
E15.5	321.17	89.08	1189.22	170.61

Table 3: Mean values and standard deviations from experimental measurements on del^{ex26} mutant mice for both dermis and epidermis.

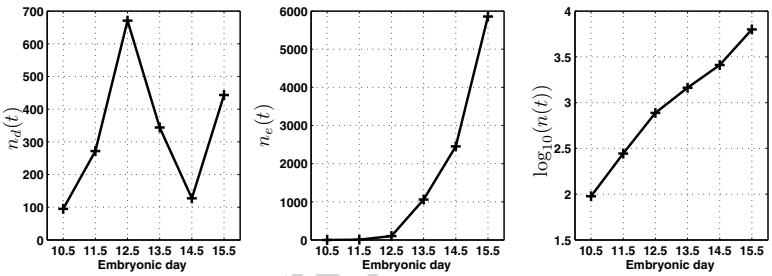

Figure 4: History of melanoblasts for $bcat^{sta}$ mice. From left to right: $n_d(t)$, $n_e(t)$ and $\log_{10}(n(t))$.

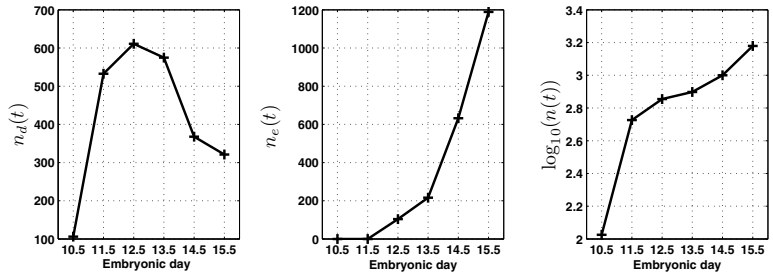

Figure 5: History of melanoblasts for del^{ex26} mice. From left to right: $n_d(t)$, $n_e(t)$ and $\log_{10}(n(t))$.

WT, $bcat^{sta}$ and del^{ex26} in particular on the position of the symmetry position and the decreasing rate of the S-shaped profile.

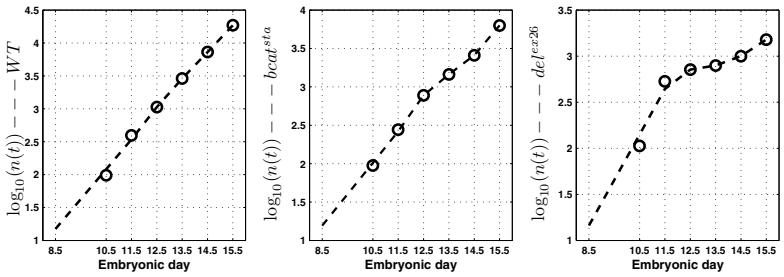

Figure 6: History of the total number of melanoblasts. From left to right: WT, $bcat^{sta}$ and del^{ex26} mice.

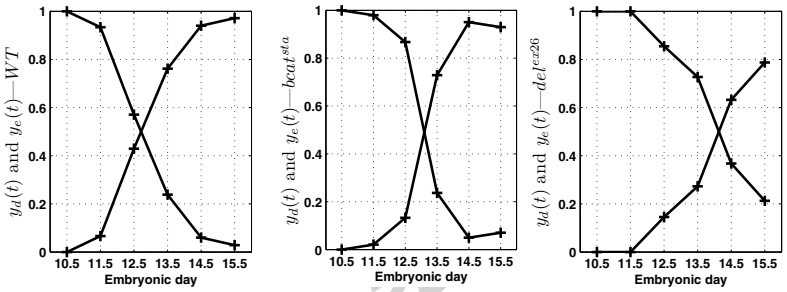

Figure 7: History of fractions of melanoblasts in dermis and epidermis. From left to right: WT, $bcat^{sta}$ and del^{ex26} mice.

2.3.3. Ratio of melanoblasts between epidermis and dermis

In may also be interesting to plot the ratio of melanoblasts between epidermis and dermis. On figure 8 the ratio for each of the mice is plotted in log scale. One can again notice a common feature shared by the three kinds of mice. In log scale the plots can be reasonably linearly regressed between embryonic days E11.5 and E14.5, showing an exponential growth of the ratio due to the combined effect of transfer between dermis and epidermis and proliferation in epidermis. One can also notice a slope break at day E14.5 for WT and $bcat^{sta}$ and even a slight decreasing of the ratio for $bcat^{sta}$. This behaviour may be explained by some feedback effects on the flux between dermis and epidermis because the ratio has reached a limit threshold. For del^{ex26} mice, the slope break does not occur maybe because the ratio still has not reached the threshold.

Below in the description of the mathematical model we will see that this ratio plays an important role in the whole dynamics of the system.

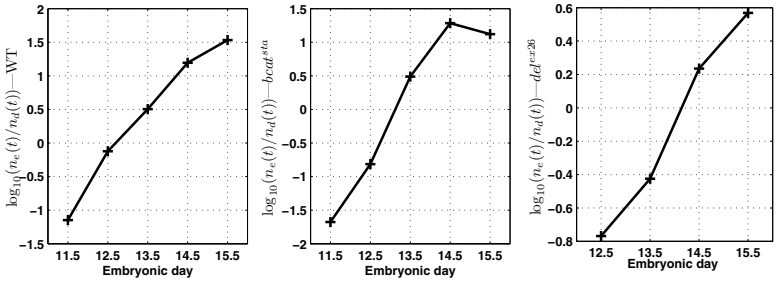

Figure 8: History of the ratio between epidermis and dermis melanoblasts. From left to right: WT, $bcat^{sta}$ and del^{ex26} mice.

3. Mathematical Models

3.1. Modeling assumptions and mathematical equations

In this section, we consider different mathematical model candidates for the proliferation dynamics. The variables $n_d(t)$ and $n_e(t)$ will respectively denote the total number of melanoblast in the dermis and in the epidermis. We will also denote $\tau_d(t)$ and $\tau_e(t)$ the doubling times in dermis and epidermis respectively and $\Phi(t) \geq 0$ the flux rate of melanoblasts from dermis to epidermis at time t. A deterministic continuous medium approach is adopted. From the biological assumptions, assuming no stochastic effect and a continuous medium, the population balance equations are

$$\frac{dn_d}{dt} = \mu_d(t)\, n_d(t) - \Phi(t, n_d, n_e), \tag{2}$$

$$\frac{dn_e}{dt} = \mu_e(t)\, n_e(t) + \Phi(t, n_d, n_e). \tag{3}$$

with

$$\mu_d(t) = \frac{\log(2)}{\tau_d(t)}, \quad \mu_e(t) = \frac{\log(2)}{\tau_e(t)}.$$

Equations (2)-(3) express the proliferation of melanoblasts at respective rates $\mu_d(t)$ and $\mu_e(t)$ and the flux $\Phi(t)$ from dermis to epidermis. The candidate models discussed below are particular choices and form of doubling times and flux. The initial condition corresponding the embryonic day E8.5, i.e. $t_0 = 8.5$, is the number of founder melanoblasts into dermis:

$$n_d(t_0) = n_{0,d}, \quad n_e(t_0) = 0. \tag{4}$$

A priori biological knowledge can give a confidence interval for the initial number of dermis melanoblasts $n_{0,d}$. Let us emphasize once again that neither biological knowledge nor experimental measurements can give information or bounds on the

quantity of flux rate Φ. This is the main difficulty and major source of uncertainty into the model.

The system (2)-(3) can be written in different forms. For example, summing up equations (2) and (3) gives

$$\frac{dn}{dt} = \mu_d n_d + \mu_e n_e \tag{5}$$

where $n = n_d + n_e$ is the total number of melanoblasts. Introducing the fractions of melanoblasts y in dermis i.e.

$$y = \frac{n_d}{n_d + n_e}, \tag{6}$$

it is easy to check that the system (2),(3) can be written in the equivalent form (for $n > 0$)

$$\frac{dn}{dt} = \left(\mu_d\, y + \mu_e\,(1-y)\right)\, n, \tag{7}$$

$$\frac{dy}{dt} = -(\mu_e - \mu_d)\, y\,(1-y) - \frac{\Phi}{n}, \tag{8}$$

The system is equation (7),(8) gives another understanding of the dynamics. Equation (7) can also be written

$$\frac{d\log(n)}{dt} = \mu(t) \tag{9}$$

with

$$\mu(t) = y(t)\mu_d(t) + (1-y(t))\mu_e(t) \tag{10}$$

which is a local exponential proliferation law with local growth rate $\mu(t)$.

Let us now derive a differential equation for the logarithm of ratio of number of melanoblasts in epidermis and dermis. If $n_d, n_e \neq 0$, equations (2) and (3) can be rewritten

$$\frac{d\log(n_d)}{dt} = \mu_d - \frac{\Phi}{n_d},$$

$$\frac{d\log(n_e)}{dt} = \mu_e + \frac{\Phi}{n_e}$$

leading to

$$\frac{d\log(n_e/n_d)}{dt} = \mu_e - \mu_d + \frac{\Phi}{y(1-y)n}. \tag{11}$$

In the previous section, it was shown that the dataset $t \mapsto \log(n_e(t)/n_d(t))$ can be reasonably regressed by a piecewise linear function. Because both $\mu_d(t)$ and $\mu_e(t)$ are seeked as bounded functions, equation (11) shows that the function

$$t \mapsto \frac{\Phi(t)}{y(t)(1-y(t))n(t)}$$

has to be a bounded function for any value of $y(t) \in [0,1]$ and $n(t) > 0$. For that reason, we will assume below that $\Phi(t)$ is in the form

$$\Phi(t) = \kappa(t)y(t)(1-y(t))n(t) \tag{12}$$

for some positive function $\kappa(t)$.

Combining both equation (8) and expression (12) gives the logistic-like equation for y

$$\frac{dy}{dt} = -c(t)y(1-y) \tag{13}$$

with

$$c(t) = \mu_e(t) - \mu_d(t) + \kappa(t). \tag{14}$$

Combining equation (11) with expression (12) also gives

$$\frac{d\log(n_e/n_d)}{dt} = c(t). \tag{15}$$

To summarize, we have the following three important equations

$$\frac{d\log(n)}{dt} = \mu(t), \tag{16}$$

$$\frac{dy}{dt} = -c(t)y(1-y), \tag{17}$$

$$\frac{d\log(n_e/n_d)}{dt} = c(t) \tag{18}$$

where $\mu = y\mu_d + (1-y)\mu_e$.

3.2. Closure

For the moment, the system is not fully closed because we do not know the functions $\mu_d(t)$, $\mu_e(t)$ and $\kappa(t)$. By (14) it is evident that the doubling times $\tau_d(t)$ and $\tau_e(t)$ are closely linked to the flux factor $\kappa(t)$. In the paper appendix, both biological interpretation and dimension of the κ function are detailed. Unfortunately, both biological knowledge and observations not sufficient to give a closed form for κ. In what follows we are going to estimate both function $c(t)$ and $\mu(t)$ from the data. This will lead to a system of variables (n, y) in closed form.

We proceed as follows: first, the functions $\log(n)$ and $\log(\frac{n_e}{n_d})$ are approximated using the spline tools with additional constraint, indeed, the curve is constrained to be an increasing function, in order that the resulting curve of $\hat{\mu}(t)$ and $\hat{c}(t)$ has a positive values. Second, the time derivatives of the functions are computed, giving estimates $\hat{\mu}(t)$ and $\hat{c}(t)$ of the functions $\mu(t)$ and $c(t)$ respectively, see figures (9), (10) and (11).

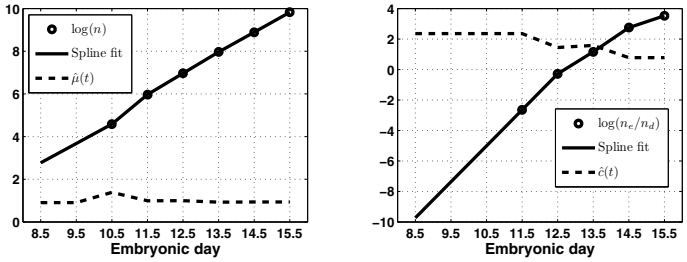

Figure 9: Estimation of the functions $\mu(t)$ and $c(t)$ for WT mice.

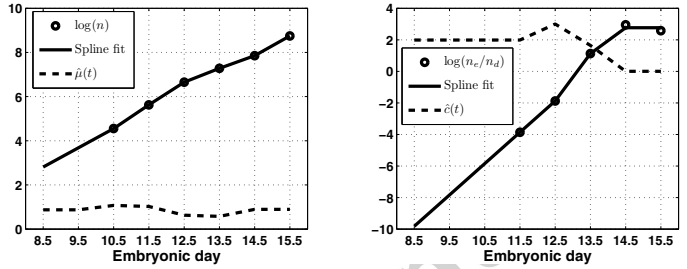

Figure 10: Estimation of the functions $\mu(t)$ and $c(t)$ for $bcat^{sta}$ mice.

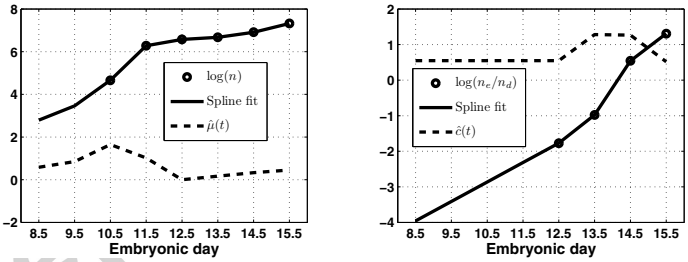

Figure 11: Estimation of the functions $\mu(t)$ and $c(t)$ for del^{ex26} mice.

Suppose that both functions $\mu(t)$ and $c(t)$ are replaced by their estimates $\hat{\mu}(t)$ and $\hat{c}(t)$ in the system. The solution of the isolated differential problem

$$\frac{dy}{dt} = -\hat{c}(t)y(1-y), \quad t \in (t_0, T], \tag{19}$$

$$y(t_0) = y_0 \tag{20}$$

(y_0 assumed to be more than one) is clearly

$$\frac{y(t)}{1-y(t)} = \frac{y_0}{1-y_0}\,\exp\left(-\int_{t_0}^{t}\hat{c}(s)\,ds\right).$$

or again

$$y(t) = \frac{y_0\,\exp(-\int_{t_0}^{t}\hat{c}(s)\,ds)}{1-y_0+y_0\,\exp(-\int_{t_0}^{t}\hat{c}(s)\,ds)}. \tag{21}$$

This gives a closed form for y once y_0 is known. Practically the initial fraction y_0 will be identified according to the biological data.

On the other hand, the solution of the differential problem

$$\frac{dn}{dt} = \hat{\mu}(t)\,n, \quad t \in (t_0, T), \tag{22}$$

$$n(t_0) = n_0 \tag{23}$$

is in form

$$n(t) = n_0 \exp\left(\int_{t_0}^{t}\hat{\mu}(s)\,ds\right). \tag{24}$$

Practically, the initial number of melanoblasts n_0 can be identified according to the biological measurements. Once $n(t)$ and $y(t)$ are computed, we get

$$n_d(t) = n(t)y(t), \tag{25}$$

$$n_e(t) = n(t)(1-y(t)). \tag{26}$$

Regarding the doubling times, from the compatibility expressions

$$\hat{c}(t) = \mu_e(t) - \mu_d(t) + \kappa(t), \tag{27}$$

$$\hat{\mu}(t) = y(t)\mu_d(t) + (1-y(t))\mu_e(t). \tag{28}$$

we get the following relations linking the growth rates to the flux factor $\kappa(t)$:

$$\mu_d(t) = \hat{\mu}(t) - (1-y(t))\,(\hat{c}(t) - \kappa(t))\,, \tag{29}$$

$$\mu_e(t) = \hat{\mu}(t) + y(t)\,(\hat{c}(t) - \kappa(t))\,. \tag{30}$$

4. The system without dependency on doubling times

Another way, from the population balance equation (2)-(3), substituting the expression (12) and taking into account (29)-(30) yields to the following mathematical model

$$\frac{dn_d}{dt} = \hat{\mu}(t)n_d(t) - \hat{c}(t)\frac{n_d(t)n_e(t)}{n_d(t)+n_e(t)}, \tag{31}$$

$$\frac{dn_e}{dt} = \hat{\mu}(t)n_e(t) + \hat{c}(t)\frac{n_d(t)n_e(t)}{n_d(t)+n_e(t)}, \tag{32}$$

$$n_d(t_0) = n_{0,d},\ n_e(t_0) = \epsilon. \tag{33}$$

For technical considerations, we assume that $n_e(t_0) = \epsilon$, with ϵ near zero. In [21], the special cases , $\hat{\mu}(t)$ and $\hat{c}(t)$ are constant functions, have been used as a model of antibiotic-resistant bacterial epidemics, where n_d and n_e are populations of nonresistant and resistant bacteria respectively, at infection age t.

Now, we consider the existence, uniqueness and behavior of solutions to problem $(31)-(33)$, in the large. In particular, we establish the estimates for stability of solutions with respect to the parameters $(n_{0,d}, n_{0,e})^T$.

Any region of the form

$$D = \{x \in \mathbf{R}^2 :\ 0 \le x_i,\ \ (i = 1, 2)\}$$

is positively invariant. This assumption will be confirmed by the following theorem. The ODEs $(31)-(33)$ can be written in the compact form as :

$$\begin{cases} \dot{x}(t) = & A(t,x), \\ x(t_0) = & x_0 \in D \end{cases} \tag{34}$$

The non-linear operator A is defined on $[t_0,\infty)\times D$, by $A = \big(A_1, A_2\big)^T$, where for all $(t,x) \in [t_0,\infty)\times D$,

$$A_1(t,x) \ = \ \hat{\mu}(t)x_1 - \hat{c}(t)\frac{x_1x_2}{x_1+x_2}, \qquad A_2(t,x) \ = \ \hat{\mu}(t)x_2 + \hat{c}(t)\frac{x_1x_2}{x_1+x_2}.$$

Our basic result is the following

Theorem 4.1. *There exists a unique solution $x_{(t_0,x_0)}(t) \in D$ of the initial value problem (34), for all $x_0 \in D$ and for all $t \ge t_0$. Moreover, if $x_0,\ z_0 \in D$ then, for all $t \ge t_0$*

$$\|x_{(t_0,x_0)}(t) - x_{(t_0,z_0)}(t)\| \le \|x_0 - z_0\| \exp\left(2\int_{t_0}^{t} \hat{\mu}(s) + \hat{c}(s)ds\right) \tag{35}$$

Proof 1. *In order to apply the result given in Theorem 5.1 [13, p. 238], we need the following results concerning the nonlinear operator A, involved in the dynamics $(31)-(33)$. Easy manipulations show that, for $x,\ y \in D$,*

$$\begin{aligned} \left|\frac{x_1x_2}{x_1+x_2} - \frac{y_1y_2}{y_1+y_2}\right| &\le \frac{x_1y_1}{(x_1+x_2)(y_1+y_2)}\,|x_2-y_2| + \frac{x_2y_2}{(x_1+x_2)(y_1+y_2)}\,|x_1-y_1|\,, \\ &\le |x_2-y_2| + |x_1-y_1| \end{aligned}$$

Then we get, for $i \neq j = (1,2)$,

$$|A_i(t,x) - A_i(t,y)| \leq (\hat{\mu}(t) + \hat{c}(t))|x_i - y_i| + \hat{c}(t)|x_j - y_j|.$$

Whence,

$$\|A(t,x) - A(t,y)\| \leq 2(\hat{\mu}(t) + \hat{c}(t))\|x - y\|. \tag{36}$$

Consequently, A *is an* $2(\hat{\mu}(t) + \hat{c}(t))$*-dissipative operator on* D *[13, p. 245]. Finally, the following subtangential condition holds: For each* $(t,x) \in [t_0, \infty) \times D$,

$$\lim_{h \to 0^+} \frac{1}{h} d(x + hA(t,x); D) = 0. \tag{37}$$

First, observe that D *is given by* $D = \prod_{i=1}^{2} D_i$ *where, for* $(i = 1,2)$,

$$D_i = \{x_i \in \mathbf{R} : \ x_i \in [0, \infty)\}$$

Let, $(t,x) \in [t_0, \infty) \times D$*, since,* $x_2 + hA_2(t,x) \in D_2$ *then,*

$$\lim_{h \to 0^+} \frac{1}{h} d(x_2 + hA_2(t,x); D_2) = 0. \tag{38}$$

Now, let $h_0 > 0$ *be sufficiently small such that* $h_0 \bar{c} \leq 1$*, where* $0 \leq \hat{c}(t) \leq \bar{c}$*, for all* $t \geq t_0$*. Then, for all* $h \in (0, h_0)$, $x_1 \left(1 - h\hat{c}(t)\frac{x_2}{x_1 + x_2}\right) \in D_1$*. Hence,* $x_1 + hA_1(t,x) \in D_1$*, whence, we have*

$$\lim_{h \to 0^+} \frac{1}{h} d(x_1 + hA_1(t,x); D_1) = 0. \tag{39}$$

Observe that,

$$d(x + hA(t,x); D) \leq d(x_1 + hA_1(t,x); D_1) + d(x_2 + hA_2(t,x); D_2)$$

and combining, the latter with $(38) - (39)$*, we get the desired result. Since* A *is a continuous function from* $[t_0, \infty) \times D$ *into* $\mathbf{R}^2$ *that maps bounded sets into bounded sets and due to the above previous results* $(36) - (37)$*, for each* $x_0 \in D$*, there is a unique solution* $x_{(t_0,x_0)} \in D$ *to (34) on* $[t_0, \infty)$*. Moreover, if* x_0, $z_0 \in D$*, the final assertion,* (35)*, follows directly from Theorem 5.1 [13, p. 238].*

5. Numerical estimation of initial fraction and number of founder melanoblasts in dermis

The next step is to validate the continuous differential model with respect to the mean data. As mentioned in the previous sections, the variables of interest are of course $n_d(t)$ and $n_e(t)$ but also $y(t)$, $n(t)$ and $n_e(t)/n_d(t)$. The open parameters y_0 and n_0 have to be identified in such a way that the solutions have to fit at best with all the variables of interest.

For the fraction of melanablasts in dermis $y(t)$ for example, we want to find the best $y_0 \in (0, 1]$ which minimizes the mean square functional

$$J_{N_m}(y_0) = \frac{1}{2}\sum_{k=0}^{N_m} \frac{(y_k^d - y_k)^2}{\sigma^2_{y_k^d}} + \frac{1}{2}\frac{\big(\log(y_0) - \log(y_0^*)\big)^2}{\sigma^2_{\log(y_0)}},$$

subject to (19)-(20), where y_k^d and $\sigma_{y_k^d}$ are, respectively, the mean fraction value and the standard deviation, computed from the measurements at embryonic day t_k. For numerical purposes, solutions of (19),(20) are discretized in time using a Runge-Kutta RK4 time advance scheme. The additional components of the cost represents the priori information term about the parameter values y_0^*. This acts to keep the logarithm of unknown initial state y_0 from deviating much more than $\sigma_{\log(y_0)}$ from $\log(y_0^*)$. Usually y_0^* is the first guess of the uncertain parameters and the starting value for the optimization procedure.
For each mouse type (WT, $bcat^{sta}$ and del^{ex26}), we have computed an initial fraction y_0. It can be noticed first that y_0 is very close to one, what is expected (the melanoblasts are in the dermis at day $E8.5$). Moreover, the results do not depend of the type of mice, what is also expected (the effects on β-catenin activation start from day E10.5). However, the constraint $n_0 \in [10, 30]$ is taken for the three types of mice. It is observed that indeed the residuals are quite small, validating the logistic-like behaviour of the fraction y. From figures 12 to 15, the fraction y and total number n profils given by the differential model, and total numbers n_d and n_e given by (25)-(26) and the ratio between epidermis and dermis $\frac{n_e}{n_d}$, are compared to the mean data. That shows a very good agreement between mean data and model.

The number of founder melanoblasts was estimated to 16.0016. Moreover, y_0 was found to be very closed to one.

Comment 5.1. *The optimal $n_{0,d}$ can be , also, obtained by minimizing the following criterion $J_{N_m}(n_{0,d})$*

$$J_{N_m}(n_{0,d}) = \frac{1}{2}\sum_{k=0}^{N_m}(z_k - x_k)^T R_k^{-1}(z_k - x_k) + \frac{1}{2}\Big(\frac{\log(n_{0,d}) - \log(n_{0,d}^*)}{\sigma_{\log(n_{0,d})}}\Big)^2 \quad (40)$$

where $x_k = (n_d(t_k), n_e(t_k))^T$ is given by the approximate discrete system of the model (31)-(33), z_k is the $(N_x \times 1)$ measurement vector and R_k is the coresponding covariance diagonal matrix

6. Uncertainty on doubling times

It appears that the equations (31)-(32) are independent of function flux factor $\kappa(t)$. But, in order to be able to estimate doubling times τ_d and τ_e, given by (29) and (30) respectively, we need the expression of this function $\kappa(t)$.

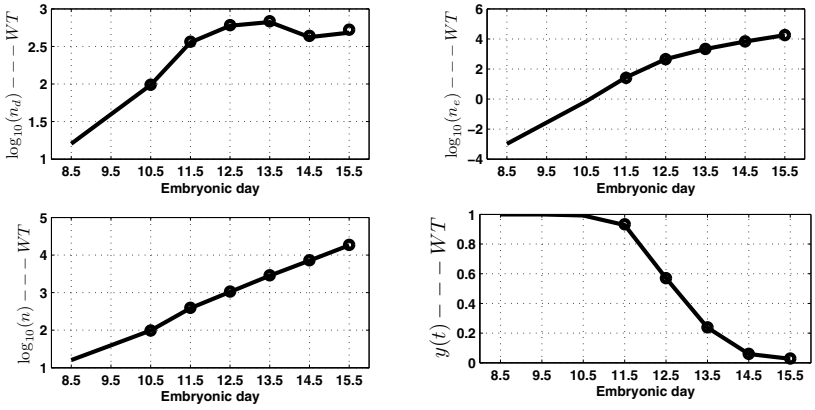

Figure 12: Comparison between data and solutions of the calibrated differential model for WT mice.

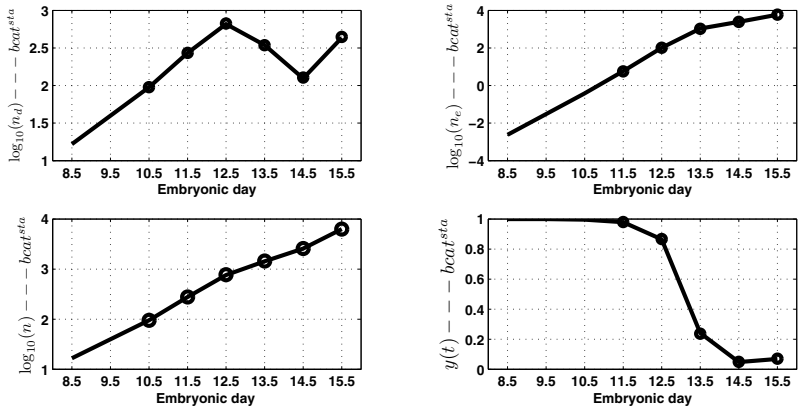

Figure 13: Comparison between data and solutions of the calibrated differential model for $bcat^{sta}$ mice.

6.1. A priori knowledge on bounds on the doubling times

Complementary biological BrdU tests performed between embryonic days E13.5 and E14.5, (Luciani et al., submitted for publication) allowed us to assume that doubling time into epidermis are smaller than doubling times into dermis, i.e.

$$\mu_e(t) \geq \mu_d(t). \tag{41}$$

It is also biologically reasonable to assume that doubling times into dermis cannot be greater than a factor (greater than one) times the doubling times into epidermis, i.e.

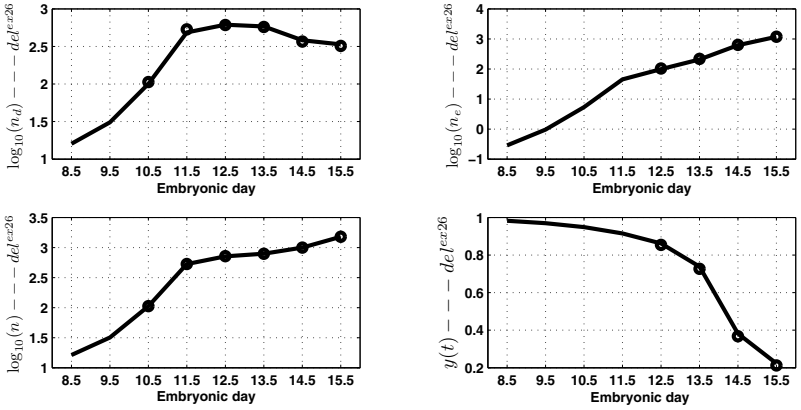

Figure 14: Comparison between data and solutions of the calibrated differential model for del^{ex26} mice.

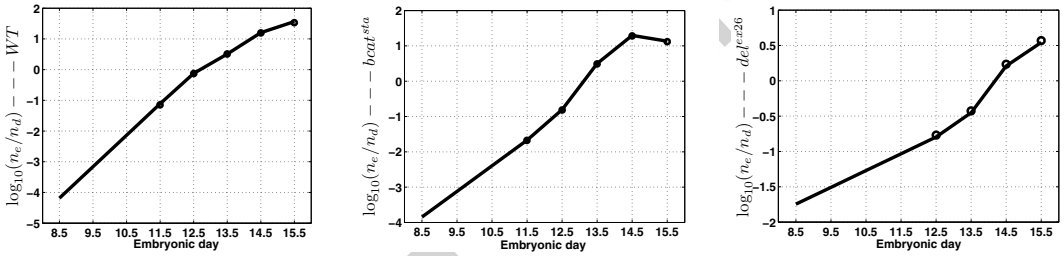

Figure 15: Comparison between data and solutions of the ratio model. From left to right: WT, $bcat^{sta}$ and del^{ex26} mice.

there is a constant $M \geq 1$ such that

$$\frac{\mu_e(t)}{\mu_d(t)} \leq M \; \forall t. \tag{42}$$

Both constraints (41) and (42) have to be taken into account in certain way. If it is assumed that $0 \leq \kappa(t) \leq \hat{c}(t)$ then we have

$$\mu_e(t) \geq \hat{\mu}(t) \quad \forall t,$$
$$\mu_d(t) \leq \hat{\mu}(t) \quad \forall t,$$

and thus the constraint (41) is satisfied.

The constraint

$$\kappa(t) \leq \hat{c}(t) \tag{43}$$

resembles a flux limiter condition. Second constraint (42) gives the inequality

$$\mu_d(t) = \hat{\mu}(t) - (1-y)[\hat{c}(t) - \kappa(t)] \geq \frac{1}{M}\,\mu_e, \tag{44}$$

or again

$$\kappa(t) \geq \hat{c}(t) - \frac{(1-\frac{1}{M})\hat{\mu}(t)}{1-y}. \tag{45}$$

Because Φ is assumed to be positive (flux from dermis to epidermis), one ask also $\kappa(t)$ to be positive. We then get the admissible range for $\kappa(t)$

$$\hat{c}(t) - \frac{(1-\frac{1}{M})\hat{\mu}(t)}{1-y} \leq \kappa(t) \leq \hat{c}(t). \tag{46}$$

6.2. Uncertainty on doubling times

Surprisingly, all the functions $\kappa(t)$ that satisfy the inequalities (46) are a priori feasible, leading to admissible doubling times that are compatible with the dynamics and satisfying the constraints (41) and (42).

That means that there is as most growth rates $\mu_d(t)$ and $\mu_e(t)$ (computed from (29)-(30)) as functions $\kappa(t)$ satisfying (46).

As a partial conclusion, the doubling times are not strictly identifiable from the data and the actual knowledge of the system. The problem of doubling time estimation is ill-posed from the deterministic point of view. The main difficulty is due to the uncertainty on the flux factor $\kappa(t)$. The robust identification of doubling times should be addressed in a probabilistic way, including a priori uncertainty on both data and model.

6.3. Coarse estimation of doubling times

In this section, we use the inequalities (46) in order to estimate the mean and the variance for $\mu_d(t)$ and $\mu_e(t)$ (computed from (29)-(30)). First, we estimated the mean and the variance of unknown function κ using the median, the lower bound ℓ_b and the upper bound u_b for κ. ℓ_b and u_b are given by

$$\ell_b(t) = \max\big(0, \hat{c}(t) - \frac{(1-\frac{1}{M})\hat{\mu}(t)}{1-y}\big), \;\; u_b(t) = \hat{c}(t).$$

The mean and the standard deviation can then be raughly estimated as

$$\bar{\kappa}(t) = \frac{\ell_b(t) + u_b(t)}{2},$$
$$S_\kappa(t) = \frac{u_b(t) - \ell_b(t)}{2}.$$

Therefore, the mean and the standard deviation for μ_d and μ_e can than be estimated as

$$\bar{\mu}_d(t) = \hat{\mu}(t) - (1 - y(t))(\hat{c}(t) - \bar{\kappa}(t)), \quad S_{\mu_d}(t) = (1 - y(t))S_\kappa(t), \quad (47)$$
$$\bar{\mu}_e(t) = \hat{\mu}(t) + y(t)(\hat{c}(t) - \bar{\kappa}(t)), \quad S_{\mu_e}(t) = y(t)S_\kappa(t). \quad (48)$$

When $(\bar{\mu_d}(t), S_{\mu_d}(t))$ and $(\bar{\mu_e}(t), S_{\mu_e}(t))$ are estimated from $(47) - (48)$, the doubling times are obtained as

$$\bar{\tau}_d(t) = \frac{\log(2)}{\bar{\mu_d}(t)}, \quad \bar{\tau}_e(t) = \frac{\log(2)}{\bar{\mu_e}(t)}$$

and the standard error of the doubling times are

$$S_{\tau_d}(t) = \frac{\log(2)}{\bar{\mu_d}(t)} - \frac{\log(2)}{\bar{\mu_d}(t) + S_{\mu_d}(t)}, \quad S_{\tau_e}(t) = \frac{\log(2)}{\bar{\mu_e}(t)} - \frac{\log(2)}{\bar{\mu_e}(t) + S_{\mu_e}(t)}.$$

From biological BrdU consideration, we take $M = 3$. The estimated mean and standard deviation doubling time were listed in Table (4)-(6).

E. day	Mean of τ_d in dermis	Std dev of τ_d in dermis	Mean of τ_e in epidermis	Std dev of τ_e in epidermis
E12.5	22.98	6.59	11.87	2.56
E13.5	26.06	8.68	15.73	1.35
E14.5	27.04	9.01	17.65	0.36
E15.5	24.62	7.03	17.44	0.14

Table 4: Mean values and standard deviations of doubling time on wild type (WT) mice for both dermis and epidermis.

E. day	Mean of τ_d in dermis	Std dev of τ_d in dermis	Mean of τ_e in epidermis	Std dev of τ_e in epidermis
E12.5	24.97	0	24.97	0
E13.5	44.74	14.91	27.01	2.33
E14.5	30.28	7.04	22.89	0.33
E15.5	17.70	0.77	16.91	0.02

Table 5: Mean values and standard deviations of doubling time on $bcat^{sta}$ mutant mice for both dermis and epidermis.

E. day	Mean of τ_d in dermis	Std dev of τ_d in dermis	Mean of τ_e in epidermis	Std dev of τ_e in epidermis
E12.5	327.25	109.08	151.19	35.51
E13.5	168.12	56.04	101.50	8.75
E14.5	74.34	24.78	48.52	0.99
E15.5	55.36	18.45	36.55	0.35

Table 6: Mean values and standard deviations of doubling time on del^{ex26} mutant mice for both dermis and epidermis.

7. Discussion, related works

The main goal of this paper was to derive a continuous-time model of mouse embryonic melanoblast proliferation dynamics which is parameterized by an activity rate of β-catenin.

The present methodology was able to return behavior, features, dependency and sensitivity with respect to some activity β-catenin at the macroscopic level.

During this work, it appeared very important to use data, not only for final parameter calibration but also for model refinement and proper derivation.

In the literature, we found a similar mathematical approach proposed in the paper by Webb [21] to analyze the dynamics of nonresistant and resistant bacteria strains in epidemic populations in hospital environments. The link between population of nonresistant bacteria and resistant bacteria present in a patient infected needs to be developed also for this type equation with flux rate in function of the fraction of two classes of bacteria (nonresistant and resistant).

We currently address two important issues of proliferation process modeling. The first issue discussed in this paper is to develop a general framework for modeling of proliferation of melanoblasts during mouse embryonic development. Second issue is to estimate the parameters of the models.

In many biological systems, inter-states cannot be directly measured in experiments. A way to overcome this shortcoming is to include uncertainty models for the states as well as for parameters seen as additional states into an augmented state space. There are today numerous robust methods of parameter estimation of nonlinear dynamic systems from partial noisy observations. The idea is to jointly estimate the states of the systems and parameters in the model.

The Extended Kalman Filter "EKF" [18, 15] for example locally performs a Kalman filter to the linearized system in the vicinity of the actual state of the system. But serious limitations are reported in the literature: linearization can be applied only if the Jacobian matrix is known. However, this is not always the case and approximate Jacobian matrices can produce unstable filters.

Recently, Julier and Uhlmann [7] have introduced a nonlinear estimation technique referred to as the Unscented Kalman Filter "UKF" which yields performance equivalent to the Kalman Filter "KF" for linear systems, yet generalizes elegantly to nonlinear

systems without the linearization steps required by the Extended Kalman Filter "EKF". This technique and its variations [19] have been used widely in Engineering and the physical sciences to estimate factor scores and parameters from noisy data.

Recently, Kolas and his coworkers[8, 9] proposed to use the Constrained Unscented Kalman Filter "CUKF" to estimate the time-varying parameters with constraint handling in the nonlinear state-space model.

The nonlinear state-space model is defined by two types of equations: state equations that define the dynamics of melanoblast proliferation dynamics through time and observation equations that describe how these state variables are observed. The general melanoblast proliferation model can be formulated as:

$$\frac{dn_d}{dt} = \mu_d(t)\, n_d - (\hat{c}(t) - \mu_e(t) + \mu_d(t))y(1-y)n, \tag{49}$$

$$\frac{dn_e}{dt} = \mu_e(t)\, n_e + (\hat{c}(t) - \mu_e(t) + \mu_d(t))y(1-y)n, \tag{50}$$

$$\frac{dn}{dt} = \hat{\mu}(t)n, \tag{51}$$

$$\frac{dy}{dt} = -\hat{c}(t)y(1-y). \tag{52}$$

The uncertain "noisy" observation model is defined as

$$z_k \quad = \quad x_k + v_k, \tag{53}$$

where $x = (n_d, n_e, n, y)^T$ and z_k is the $(N_x \times 1)$ measurement vector, v_k is the measurement noise with zero mean and covariance matrix

$$R(k) = diag(\sigma_{n_d}(k)^2; \sigma_{n_e}(k)^2; \sigma_n^2(k); \sigma_y^2(k)).$$

Note that the estimation of doubling times may be solved under some constraints. These constraints can be handled by several ways, for instance by identifying the natural logarithms of the parameters. The EKF and CUKF can be used to estimate the parameter $\theta(t) = (\log(\mu_d(t)), \log(\mu_e(t)))^T$, together with the system state $(49) - (52)$. We add, to the model $(49) - (52)$, the system equation:

$$\frac{d\log(\mu_d(t))}{dt} = 0,$$

$$\frac{d\log(\mu_e(t))}{dt} = 0.$$

Thus will be at the aim of a future paper.

8. Concluding remarks

In this paper, a mathematical model of melanoblast proliferation process during mouse embryonic development is proposed.

The mathematical model describes the evolution of total number of melanoblasts in both dermis and epidermis between embryonic development days E8.5 and E15.5. The developed methodology is a compromise between expected balance equations, behaviors and feature extraction from data, verification of data fitting. During the design of the model, a set of a priori biological informations have also been taken into account (parameter bounds, interval on ratio of doubling times, etc.).

Three datasets of melanoblast populations corresponding to Wild Type mice, and two mutant mice with different β-catenin activity are used. The unknow initial number of founder melanoblasts in the dermis at E8.5 has been identified from biological measurements provided in [3]. As a result, the present model is able to fit with the mean data very well for the three kinds of mouse lines. In this paper, it is also shown that the doubling times cannot be identified from the actual experimental observations from the deterministic point of view.

Future work is aimed at considering doubling times and observations as uncertain variables (random variables). This will allow us to use robust parameter identification algorithms like Unscented Kalman Filter or particle filters for robust estimation of doubling times (for further detail see Section 7).

Another open question today is the study of the impact of β-catenin activation level on the migration process (speed of migration, spatial patterns), for more detail, a numerical algorithm to simulate chemotactic and/or diffusive migration on a one-dimensional growing domain is developed in [17].

Appendix A. Flux, flux speed and κ function

In this appendix we give a better understanding of what is the dimension and meaning of the κ function and its link with the cell moving velocity from dermis to epidermis. Assume that the mouse trunk is idealized as a cylinder of length $L(t)$ and radius $r(t)$ at embryonic instant t. Assume also that the thickness of the dermis is $\delta r(t) \ll r(t)$. The volume occupied by the dermis is

$$V(t) = \pi[(r(t) + \delta r(t))^2 - r^2(t)]L(t) \approx 2\pi r(t)\delta r(t)L(t).$$

Suppose that the density $\rho_d(t)$ of melanoblasts in the dermis is spatially homogeneous. Then we get

$$\rho_d(t) = \frac{n_d(t)}{V(t)}.$$

The membrane surface between dermis and epidermis is equal to

$$S(t) = 2\pi r(t)L(t).$$

Thus, if $u(t)$ the spatial velocity of melanoblasts from dermis to epidermis in the normal direction of the membrane, the total flux of melanoblasts through the membrane is equal to

$$\begin{aligned} \Phi(t) &= S(t)\rho_d(t)u(t) \\ &= \delta r(t)u(t)n_d(t). \end{aligned}$$

From the other script

$$\Phi(t) = \kappa(t)y(t)(1 - y(t))n(t),$$

one obtains

$$\kappa(t) = \frac{\delta r(t)}{1 - y(t)}\, u(t). \tag{A.1}$$

The function $\kappa(t)$ depends on the velocity of cells but also on the thickness of the dermis. Expression (A.1) makes us think that the function $\frac{u(t)}{1-y(t)}$ has to be bounded. Unfortunately, the biological knowledge is not sufficient to give a closed form to (A.1).

Acknowledgements

This work is partly funded by the Consortium Institut Carnot Centrale-Supélec "Sciences des Systèmes C3S", `http://www.supelec.fr/d2ri/c3s/`.

References

[1] Bellomo, N., Li, N. K. and Maini, P. K., 2008. *On the Foundations of Cancer Modelling: Selected Topics, Speculations, and Perspectives*. Math. Mod. Meth. Appl. Sci. 18, 593–646.

[2] Bellomo, N. and Forni, G., 2008. *Complex multicellular systems and immune competition: New paradigms looking for a mathematical theory,* Current Top. Develop. Biol. 81, 485–502.

[3] Delmas, V., Beermann, F., Martinozzi, S., Carreira, S., Ackermann, J., Kumasaka, M., Denat, L., Goodall, J., Luciani, F., Viros, A., Demirkan, N., Bastian, B. C., Goding, C. R. and Larue, L., 2007. *β-catenin induces immortalization of melanocytes by suppressing $p16^{INK4a}$ expression and cooperates with N-Ras in melanoma development*. Genes and development, 21, 2923–2935.

[4] Denat, L. and Larue, L., 2007. *Le mélanome malin cutané et le rôle de la protéine paradoxale Microphthalmia transcription factor*. Bull Cancer, 94, 81–92.

[5] Gatenby, R. A., Vincent, T. L. and Gillies, R. J. 2005. *Evolutionary dynamics in carcinogenesis*, Math. Mod. Meth. Appl. Sci. 15, 1619–1638.

[6] Hanahan, D., and Weinberg, R. A., 2000. *The Hallmarks of Cancer*. Cell, 100, 57–70.

[7] Julier, S. J., Uhlmann, J. K. and Durrant-Whyte, H. F., 1995. *A new approach for filtering nonlinear systems*. In Proceedings of the American Control Conference, Seattle, Washington: IEEE, 1628–1632.

[8] Kolas, S., Foss, B. A. and Schei, T. S., 2009. *Constrained nonlinear state estimation based on the UKF approach*. Computers and Chemical engineering, 33, 1386–1401.

[9] Kolas, S., Foss, b. A. and Schei, T. S., 2009. *Noise modeling concepts in Nonlinear State Estimation*. Journal of Process Control, 19, 1111-1125.

[10] Komarova, N. L., 2006. *Spatial Stochastic Models for Cancer Initiation and Progression*. Bull. Math. Biol., 68, 1573–1599.

[11] Komarova, N. L., 2007. *Stochastic modeling of loss- and gain-of-function mutation in cancer*. Math. Mod. Meth. Appl. Sci. 17, 1647–1674.

[12] Larue, L. and Delmas, V., 2006. *The WNT/Beta-catenin pathway in melanoma*. Frontiers in Bioscience, 11, 733-742.

[13] Martin, R.H. Jr., 1976. *Nonlinear Operators and Differential Equations in Banach Spaces*. Wiley, New York.

[14] Michor, F., Iwasa, Y. and Nowak, M. A. , 2004. *Dynamics of cancer progression*, Nature Rev. Cancer 4, 197–205.

[15] Poignet, Ph. and Gautier, M., 2000. *Comparison of weighted least square and extended Kalman filtering methods for dynamic identification of robots*. Pro. of the 2000 IEEE, Int. Conf. on Robotics & Automation, SF, CA., 4, 3622–3627.

[16] Silver, D. L., Hou, L., Somerville, R., Young, M. E., Apte, S. S., and Pavan, W. J., 2008. *The secreted metalloprotease ADAMTS20 is required for melanoblast survival*. PLoS Genetics, 4(2):e1000003.

[17] Simpson, M. J., Landmana, K. A. and Newgreen, D. F., 2006. *Chemotactic and diffusive migration on a nonuniformly growing domain: numerical algorithm development and applications*. J. Comput. Appl. Math. , 192, 282–300.

[18] Sorenson, H. W., 1985. *Kalman filtering: theory and application*. IEEE Press.

[19] Wan, E. and Van der Merwe, R., 2001. *The Unscented Kalman Filter*. In S. Haykins (Ed.), Kalman filtering and neural networks, New York: Wiley, 221–280.

[20] Webb, G. F., 1985. *Theory of Nonlinear Age-Dependent Population Dynamics*. Marcel Dekker, New York.

[21] Webb, G. F., D'Agata, E. M. C., Magal, P. and Ruan, S., 2005. *A Model of antibiotic-resistant bacterial epidemics in hospitals*. Proc Natl Acad Sci U S A., 102(37), 13343–13348.

[22] Yajima, I., Belloir, E., Bourgeois, Y., Kumasaka, M., Delmas, V. and Larue, L., 2006. *Spatiotemporal Gene Control by the Cre-ERT2 System in Melanocytes*. Genesis, 44, 34–43.